Layer-Dependent Modulation of Tungsten Disulfide Photoluminescence by Lateral Electric Fields

Zhengyu He,[†] Yuewen Sheng,[†] Youmin Rong,[†] Gun-Do Lee,[‡] Ju Li,[§,∥] and Jamie H. Warner*[,†]

[†]Department of Materials, University of Oxford, Parks Road, Oxford OX1 3PH, United Kingdom, [‡]Department of Materials Science and Engineering, Seoul National University, Seoul 151-742, Republic of Korea, and [§]Department of Nuclear Science and Engineering and [∥]Department of Materials Science and Engineering, Massachusetts Institute of Technology, 77 Massachusetts Avenue, Cambridge, Massachusetts 02139, United States

ABSTRACT Large single-crystal domains of WS_2 are grown by chemical vapor deposition, and their photoluminescent properties under a lateral electric field are studied. We demonstrate that monolayer and bilayer WS_2 have opposite responses to lateral electric fields, with WS_2 photoluminescence (PL) substantially reduced in monolayer and increased in bilayers with increasing lateral electric field strength. Temperature-dependent PL measurements are also undertaken and show behavior distinctly different than that of the lateral electric field effects, ruling out heating as the cause of the PL changes. The PL variation in both monolayer and bilayer WS_2 is attributed to the transfer of photoexcited electrons from one conduction band extremum to another, modifying the resultant recombination pathways. This effect is observed in 2D transition metal dichalcogenides due to their large exciton binding energy and small energy difference between the two conduction band extrema.

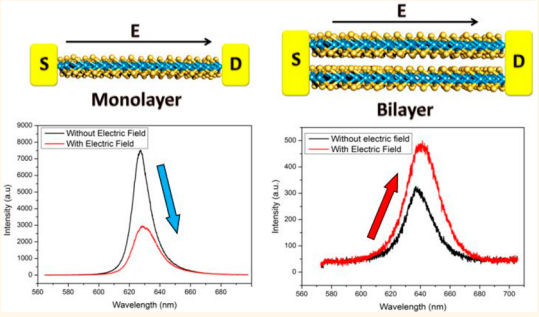

KEYWORDS: WS_2 · transition metal dichalcogenides · tungsten disulfide · optoelectronics · 2D crystals · photoluminescence

Atomically thin transition metal dichalcogenides (TMDs) are 2D materials that consist of two hexagonal planes of chalcogen atoms X (S, Se) bonded to transition metal atoms M (Mo, W) arranged hexagonally. Bulk TMDs play an important role as dry lubricants and have properties different than those of 2D monolayer and few-layer thin films.[1] Two-dimensional TMDs have unique electrical and optical properties, evolving from an indirect to a direct band gap when the number of layers decreases down to a monolayer.[2−5] The very large exciton binding energy, due to the 2D nature,[6] leads to strong photoluminescence (PL) at room temperature.[7−10] The 2D TMD materials have potential applications in a variety of optoelectronic devices, including photodetectors,[11−13] solar cells,[14−17] light-emitting devices,[16,18,19] and phototransistors.[20,21]

For many applications, engineering the optical properties *via* external modulation is highly desired.[8] Tongay *et al.* reported that crossover from an indirect to a direct band gap can be thermally driven in $MoSe_2$, where heating induced larger interlayer spacing.[8] Strain induces lattice parameter changes and modulates the band structure, altering the optical properties of WSe_2.[22] A more desirable way to control the optical properties is through electrical manipulation. Electrostatic charging in a field effect transistor can charge the neutral exciton and produce different emission spectra.[23,24] Density functional theory (DFT) calculations also predict that sufficiently high vertical electric fields can bring the conduction and valence bands closer or even transform TMDs from semiconductors to zero-gap materials.[25] However, few reports have explored the optical response of TMDs under a lateral electric field, which has been proven to be an effective method to manipulate the optical properties of many other materials. Bludau *et al.*[26] and Skromme *et al.*[27] reported PL quenching from bulk GaAs and InP and attributed it to impact ionization. Similar measurements have also been carried out on low-dimension materials. Zhang *et al.*[28] observed field-induced PL quenching on $Al_{0.3}Ga_{0.7}As/GaAs/Al_{0.3}Ga_{0.7}As$

* Address correspondence to jamie.warner@materials.ox.ac.uk.

Received for review November 19, 2014 and accepted February 13, 2015.

Published online February 23, 2015
10.1021/nn506594a

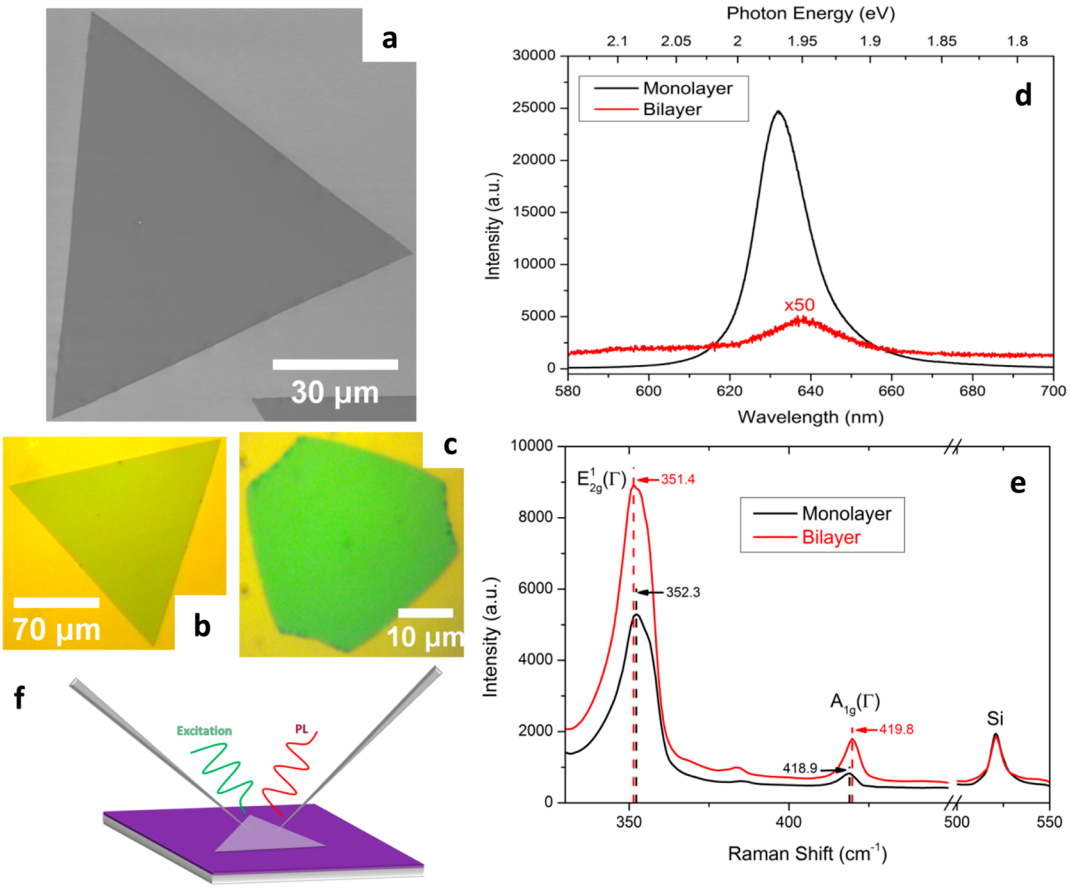

Figure 1. Identification of monolayer and bilayer WS_2. (a) SEM image of monolayer single-crystal triangular-shaped WS_2 domain. (b,c) Optical image of (b) monolayer (triangle) and (c) bilayer (hexagon) WS_2. (d) Photoluminescence spectra of monolayer and bilayer WS_2. (e) Raman spectra of monolayer and bilayer WS_2. Black line: monolayer. Red line: bilayer. (f) Schematic diagram of the setup used in the experiment to measure PL under a lateral electric field.

single quantum wells with ultrahigh time response, opening up the possibility of quantum-well-based high-speed optical modulators. Again, impact ionization has been proposed to be the dominant quenching mechanism. Huang *et al.*[29] have reported PL switching from single colloidal quantum dots using an electric field and argued that direct exciton ionization was the dominant mechanism. Field-induced PL quenching was reported for quantum nanorods, explained by a diminishing transition matrix element.[30]

Here we examine the changes to photoluminescence spectra from monolayer and bilayer WS_2 when a lateral electric field is applied. For monolayer WS_2, increasing the lateral electric field leads to PL quenching, while for the bilayer it causes an increase in PL emission. This finding can help develop more efficient optoelectronic devices based on 2D TMD materials.[31−33] Possible mechanisms behind the PL quenching and enhancement are discussed.

RESULTS AND DISCUSSION

Large 2D single crystals of WS_2 were grown by chemical vapor deposition (CVD) on Si substrates with a 300 nm oxide layer using our previously reported method.[34] This results in primarily monolayer domains, but some bilayer and few-layer domains can also be found within the sample. Figure 1a shows a scanning electron microscopy (SEM) image of the monolayer single-crystal WS_2 domain with an average size of about 100 μm. Monolayer and bilayer WS_2 domains can be distinguished by optical contrast if the RGB channel of the imaging CCD is optimized.[18] Figure 1b,c shows the optical microscopy images of monolayer (triangle) and bilayer (hexagon) isolated domains. Monolayer and bilayer are further confirmed by their PL signal, presented in Figure 1d. Under the same excitation laser power and CCD acquisition time, the integrated PL intensity from the monolayer is about 200 times stronger than that from the bilayer region, due to the emergence of indirect band gap transitions in bilayer WS_2 and the direct band gap transition for monolayer WS_2.[10,35] Raman spectroscopy can also help in determining single-layer from bilayer and few-layer WS_2, shown in Figure 1e. The black line represents the Raman spectrum from monolayer WS_2, showing $E_{2g}{}^1$ and A_{1g} phonon modes at 352.3 and 418.9 cm^{-1}. Bilayer WS_2 has a different Raman spectrum (red line in Figure 1e), with $E_{2g}{}^1$ blue-shifting to 351.4 cm^{-1} and A_{1g} red-shifting to 419.8 cm^{-1}, consistent with what has been previously reported.[10,36] A less prominent

peak around 380 cm^{-1} originates from the symmetry assignment $2LA(M) + 2E_{2g}{}^{2}(M)$[37] (LA is the longitudinal acoustic phonons; M refers to the specific direction and magnitude of the momentum q of the phonon and in the phonon dispersion; they appear at the M point of the Brillouin zone).

Figure 1f depicts the schematic diagram of the experimental setup used to monitor the PL spectra under different lateral electric fields by applying a source-drain bias. Lithographic patterning to make electrodes to the WS_2 was avoided to ensure that no defects or contamination were introduced by processing the as-grown WS_2 that could influence its PL response.[24] Source-drain electrodes were made by positioning two ultrafine tungsten tips directly onto the surface of the WS_2 domains using micromanipulators, resulting in stable contacts. The tungsten tips were typically positioned 20 μm apart underneath a long working distance objective lens in a PL confocal microscope with an attached spectrometer. The PL was excited in the middle of the two electrodes using a 532 nm laser focused to $\sim$2 μm spot. Although the misalignment between the WS_2 conduction band and the work function of the tungsten tips can introduce a Schottky barrier, it is still possible to study the effects of biasing in this system.

Figure 2a,b shows the typical PL behavior of monolayer WS_2 under an external lateral electric field by applying a source-drain bias. We repeated these measurements on numerous monolayer crystals, which all showed similar qualitative behavior. Under low electric field, minimal current flows and the PL changes little. However, when the electric field exceeds a certain value, such as 1 kV/cm in this case, the intensity of PL starts to decrease dramatically up to 50% of the original value as the electric field continues to increase. Applying a higher electric field can quench the PL up to 83% of the zero-field value (Supporting Information S3). It also shows reversible behavior where the PL intensity goes back to the original value as the electric field returns to zero. This indicates that the PL quenching observed under an electric field is not caused by permanent structural changes or chemical reactions with species in the air. There is a small difference in the rate of PL change with forward and reverse sweeps of the electric field, probably due to charging effects, but the main purpose of Figure 2c is to show the reversibility of the PL modulation. In addition to the PL quenching effect, another feature shown in Figure 2a,b is the small red shift of PL spectra under an electric field, which will be discussed in detail in the next section. Figure 2c,d shows both traces of PL integrated intensity and source-drain current *versus* a lateral electric field. The nonlinearity of the $I-V$ curve arises from the Schottky barrier, due to the misalignment between the work functions of the source-drain electrodes and the WS_2 conduction band.[38] In some other cases, two different quenching rates are observed (Supporting Information S1). Once the electric field exceeds threshold but with minimal current flowing, PL starts quenching with relative low rate. Further increasing the electric field leads to the onset of current flowing, followed by PL quenching with high rate, indicating that the PL quenching process is related not only to the electric field but also to the current flowing in the material. In Figure 2e, we plot the integrated PL intensity *versus* source-drain current to find the correlation between current and PL intensity. With minimal current flow, PL intensity shows fluctuations within a small range, which is then followed by a drastic quenching process. With current increasing continuously, the quenching rate decreases gradually.

The behavior of bilayer WS_2 under a lateral electric field is completely different than the monolayer case, with the PL greatly enhanced, as illustrated in the PL spectra in Figure 3a and contour color map in Figure 3b. Similar to the monolayer case, the PL intensity does not change much under a weak electric field, where the current is small. As the field strengthens to a certain threshold value (2.0 kV/cm in this case), the PL signal starts increasing substantially up to 150% of the original value. We have repeated these measurements on more than 10 different samples to confirm the consistency of the behavior. Again, the reversibility of this behavior eliminates the possibility of permanent structural change or chemical reaction caused by the electric field and current flowing through the material. Apart from intensity changes, the electric field also red shifts and broadens the PL peak slightly. Figure 3c plots the integrated PL intensity *versus* electric field, enabling us to explore the PL intensity change in detail. A noteworthy phenomenon is that the PL first undergoes quenching if the electric field reaches a threshold value (1.25 kV/cm in this case) prior to enhancement. Such coexistence of both quenching and enhancement indicates two competing mechanism behind the PL change. The $I-V$ relationship is plotted in Figure 3d, where the nonlinearity is attributed to the Schottky barrier between the W electrode and WS_2. Figure 3e shows the correlation between PL intensity and source-drain current. It starts with fluctuations within a limited range under a very small current flow. The increasing current first concurs with PL quenching and is then followed by enhancement. The enhancement rate slows and stabilizes at a constant value with ascending current.

We measured how the PL changes for monolayer and bilayer WS_2 as a function of temperature in order to explore whether joule heating is the cause for the observed PL effects. Prior work on $MoSe_2$ showed that high temperature quenched the PL of monolayer $MoSe_2$ while it enhanced the PL of multilayer $MoSe_2$.[8] Figure 4a,b shows the temperature-dependent PL of monolayer WS_2. Clearly, Figure 4a indicates that

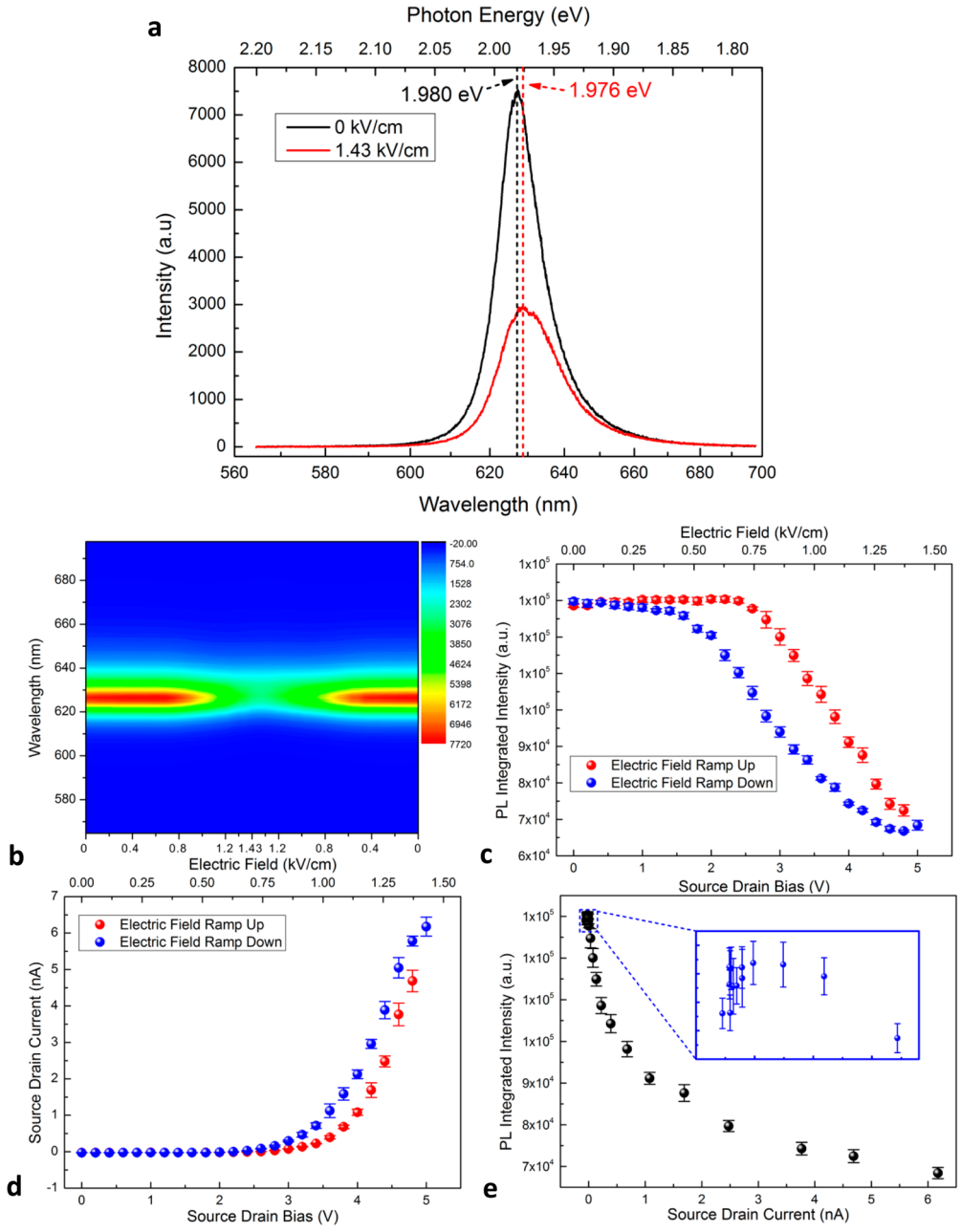

Figure 2. PL of monolayer WS_2 under lateral electric field. (a) Typical PL spectra under two different electric fields, 0 and 1.43 kV/cm. Quenching effect and red shift can be clearly observed. (b) Color contour map of PL spectra under a lateral electric field. (c) PL integrated intensity *versus* electric field. (d) *I*–*V* trace during laser illumination and PL measurement. Red dots: electric field ramps up. Blue dots: electric field ramps down. (e) Correlation between the integrated PL intensity and the source-drain current during the bias ramping up. Inset: magnified image of the area labeled with a blue rectangle.

increasing temperature quenches the PL dramatically by about 40% of the room temperature intensity. This quenching effect is due to the nonradiative electron–hole recombination rate increasing exponentially with increasing temperature.[39] However, increasing the temperature of the bilayer domain decreased the PL to ~48% of the original intensity, shown in Figure 4c,d, opposite to what we have observed for WS_2 bilayers under an electric field in Figure 3. We repeated these measurements more than 10 times on different samples to ensure their consistency and validity. Therefore, there must be another mechanism responsible for the PL enhancement of bilayer WS_2 induced by an electric field. Along with quenching, the PL peaks in both monolayer and bilayer WS_2 experience a large red shift with increasing temperature, as shown in Figure 4b,d. Such behavior is similar to the response of conventional semiconductors under high temperature, which result from increased electron–phonon interactions and slight changes in bonding lengths. Thus, it provides a method to evaluate the temperature of a semiconductor.[40] By employing a

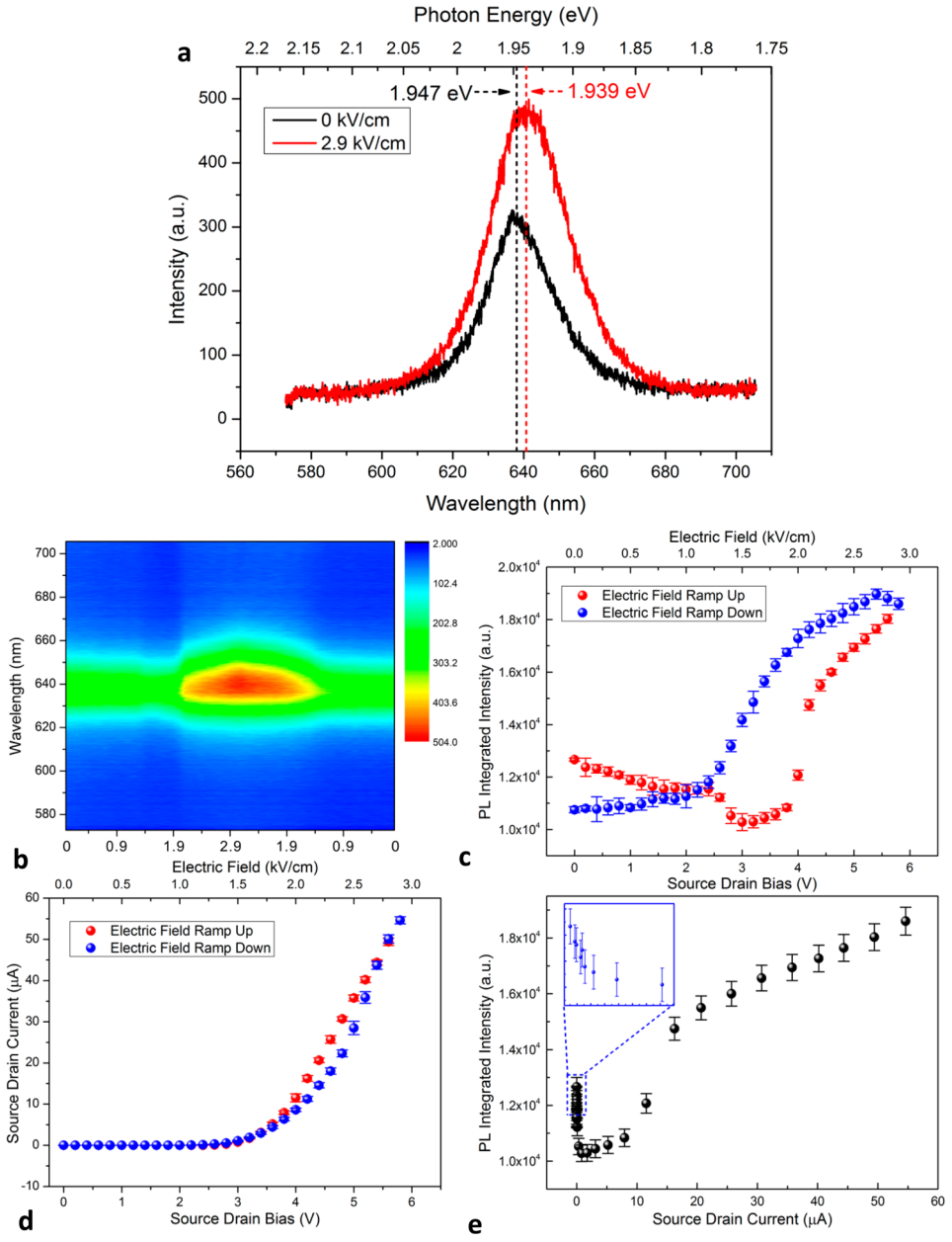

Figure 3. PL signal from bilayer WS_2 under different lateral electric field. (a) Typical PL spectra under an electric field of 0 and 2.9 kV/cm. (b) Color contour map of PL spectra under a lateral electric field. (c) Integrated PL intensity *versus* electric field. (d) *I*−*V* trace under laser illumination and during PL measurement. Red dots: electric field is ramped up. Blue dots: electric field is ramped down. (e) Correlation between integrated PL intensity and source-drain current during the process of bias ramping up. Inset: magnified image of area labeled with a blue rectangle.

standard expression for the dependence of the semiconductor band gap *versus* temperature,[41] it is possible to obtain the expression for exciton emission energy as a function of temperature, as in eq 1:[24,42]

$$E(T) = E_0 - S\langle\hbar\omega\rangle\left[\coth\left(\frac{\langle\hbar\omega\rangle}{2k_BT}\right) - 1\right] \quad (1)$$

where E_0 is the emission energy at zero absolute temperature, S is a dimensionless coupling constant, and $\langle\hbar\omega\rangle$ is the average phonon energy. At room temperature for monolayer WS_2, the best fitting yields E_0 = 2.08 eV, S = 2.47, and $\langle\hbar\omega\rangle$ = 13.0 meV, and for bilayer, E_0 = 1.97 eV, S = 2.70, and $\langle\hbar\omega\rangle$ = 10.8 meV. With the help of this expression, it is possible to derive the temperature difference of WS_2 under different electric fields in the region where the PL is being measured by comparing the emission energy difference.[40] In Figures 2a and 3a, the emitted photon energy shifts 4 meV for monolayer and 8 meV for bilayer, toward the low-energy region, corresponding to a temperature increase of 15 and 29 K, respectively. Such a temperature change can only yield a PL intensity suppression of about 6.0% for monolayer and 6.5% for bilayer, which is

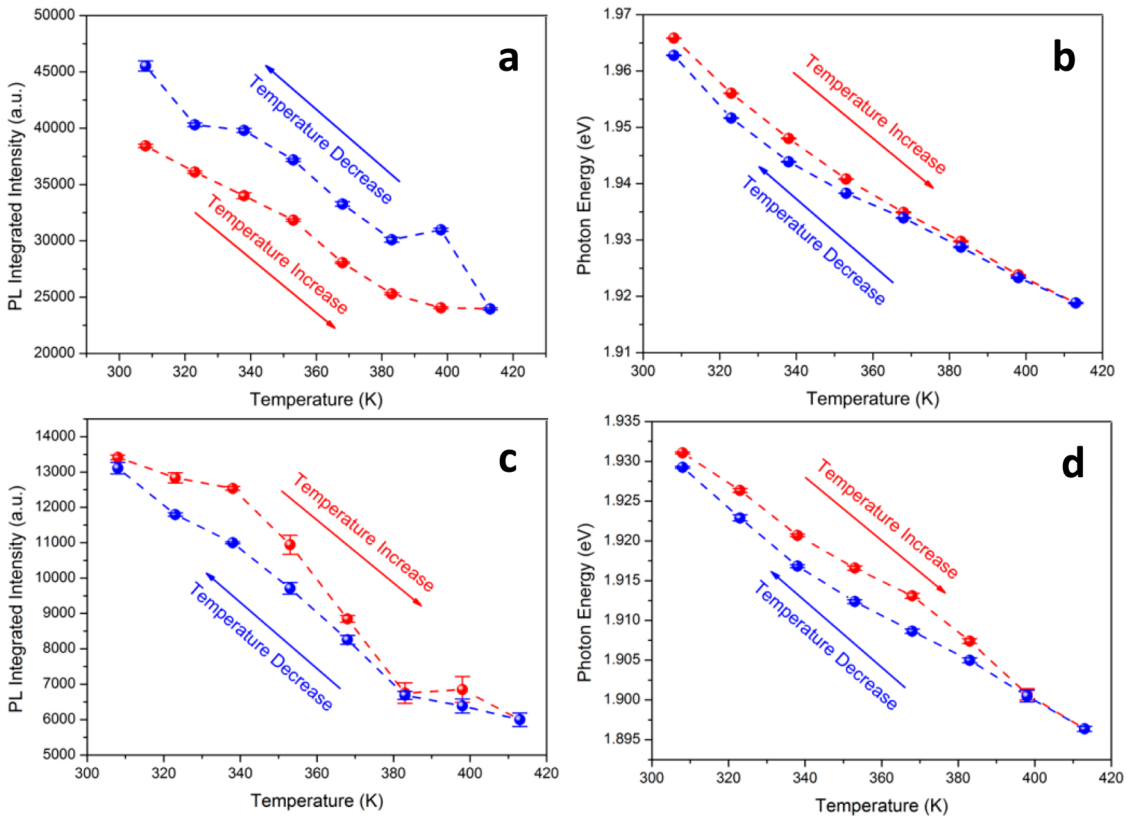

Figure 4. Temperature-dependent PL of WS_2. (a,b) Monolayer. (c,d) Bilayer. (a,c) Integrated PL intensity *versus* temperature. (b,d) PL photon energy *versus* temperature. Red line: temperature increase. Blue line: temperature decrease.

much smaller than the PL variations observed in Figures 2 and 3. Therefore, it is unlikely that temperature effects are the dominant factor causing changes in the electric-field-dependent PL measurements.

We now discuss various mechanisms that can lead to PL variation under an electric field. According to previous reports, possible causes of PL quenching include (a) thermal effects,[8] (b) Auger decay,[43] (c) direct exciton ionization,[29] and (d) impact ionization.[26,27] Thermal effects can be excluded here because we performed the temperature-dependent PL measurements and showed that this cannot account for the observed PL changes of both monolayer and bilayer WS_2 under an electric field. Because the electric field causes brightening of the PL in the bilayer WS_2 quenching processes such as Auger decay, direct exciton ionization and impact ionization cannot solely explain the behavior in both monolayer and bilayer WS_2. Auger decay has been shown to limit electroluminescent emission of light-emitting diodes,[43] but it is only significant under very high carrier densities,[43,44] especially for a wide band gap semiconductor.[45] For direct exciton ionization by the electric field, we can calculate the exciton ionization threshold field strength, which is approximately given by $E_{ex}/e \times a_{ex}$, where E_{ex} is the binding energy of the exciton, e is the charge unit, and $a_{ex} = (m_0/\mu)\epsilon_r a_B$ is the exciton radius where m_0 is electron rest mass, μ is reduced effective mass of exciton, ϵ_r is the relative dielectric constant, and a_B is the Bohr radius.[46] Since the applied electric field is along the in-plane direction, we only need to consider the in-plane component of these parameters. For monolayer WS_2, $E_{ex} = 0.28$ eV,[47] $\mu_{xy} = 0.16m_0$,[47] and $\epsilon_{r,xy} = 13$.[47] This yields a threshold electric field of about 6×10^5 V/cm, which is 2 orders of magnitude higher than the experiment value ($\sim 10^3$ V/cm, Figure 2b,c). For the bilayer, the exciton binding energy of bilayer WS_2 is about one-half that of monolayer WS_2, while the reduced mass and dielectric constant change little.[6,18] Hence the threshold field strength of direct exciton ionization is about 10^5 V/cm, which is still too high compared with that used in our experiment (1.25×10^3 V/cm, Figure 3b,c). Therefore, direct exciton ionization is unlikely to account for the electric-field-induced quenching we observe in monolayer WS_2.

The extremely large exciton binding energy in WS_2 for both monolayer and bilayer means that impact ionization is unlikely to occur within the experimental parameters we used. When the kinetic energy of charge carriers is high enough, they can ionize the photogenerated excitons through the collision process, which modifies the resultant PL recombination pathways. Although there is a possibility that the energy of a very small amount of electrons may exceed the binding energy due to the energy distribution, it is unlikely to be the main contributor to PL

quenching. Therefore, impact ionization is unlikely to be the dominant factor for PL quenching in monolayer WS_2.

Modification to the band structure of bilayer WS_2 by an electric field requires electric field strengths much higher than those we utilize in our measurements.[25] Typically, electric fields are applied perpendicular to the plane of the WS_2, and large electric field strengths can be generated due to the ultrathin nature of the WS_2 and the ability to have small separation between electrodes. In our devices, the electrodes are laterally positioned and have large distance scales between electrodes, limiting the ability to reach ultrahigh electric field strengths necessary for band structure modification.

A change in the PL emission from both monolayer and bilayer WS_2 is most likely due to modifications in the recombination pathways associated with population changes of photoexcited electrons in the conduction band minima. A change in the level occupancy factors of the K−K direct recombination pathway is likely to lead to the major PL quenching in monolayer WS_2 and an increase in bilayer WS_2. Electrons in an n-type semiconductor with two conduction band extremum can transfer from the first extremum to a secondary one under an electric field,[48,49] and we propose that the quenching in Figure 2 can possibly originate from the transfer of photoexcited electrons from the conduction band minimum at the K point to the secondary extremum (middle point between K and Γ), which modifies the electron distribution between these two conduction band extremum. It will decrease the level occupancy factors of the K−K direct recombination pathway. The energy difference between two extrema is about 70 meV (derived from DFT-calculated band structure),[50] smaller than the binding energy of the exciton. Negative differential resistance is absent here, which we attribute to the very close electron effective mass between these two conduction band extrema.[48] A similar phenomenon can also help explain the PL enhancement in bilayer WS_2, where the transfer of some photoexcited electrons from the conduction band minimum (middle point between Γ and K) to the secondary extremum (K point) will increase the level occupancy factors of the K−K direct recombination pathway. In bilayer WS_2, the energy difference between the two extrema is 85 meV and still below the exciton binding energy.[51]

Electron transitions between the two extrema in the conduction band require both energy and momentum change. The absorption of a photon initially creates an exciton, which is charge-neutral and therefore should not experience a significant drift velocity under the lateral electric field. Two physical processes related to a lateral electric field that could cause changes to photoexcited excitons are scattering by energetic mobile charge carriers accelerated under the lateral electric field (*i.e.*, interactions with conduction electrons from the flowing current) and the formation of charge excitons (trions) that are common in WS_2 grown on SiO_2 surfaces. Trions will be accelerated by the lateral electric field and may scatter from defects, impurities, and surface adsorbates. Considering that PL changes coincided strongly with the onset of current flow in the WS_2, we believe that interactions with energetic mobile charge carriers is the likely physical process that causes energy and momentum shifts in the photogenerated excitons.

CONCLUSION

In summary, the application of a lateral electric field leads to the modulation of the PL properties of WS_2. Photoluminescence from monolayer WS_2 can be quenched, while the emission ability of the bilayer can be enhanced. Electron transfer between two points in the conduction band is proposed as a possible mechanism behind the field-dependent PL variations. This is due to the unique band structure (small energy difference between two conduction band extrema) and the very large exciton binding energy in 2D WS_2. In conventional bulk semiconductors, it is very hard to observe the effect of this physical process on the luminescent properties because the energy difference between the conduction band extrema is much larger than the exciton binding energy.[52] Further work will focus on understanding the specific details of the mechanisms that lead to the PL changes in both monolayer and bilayer. These results not only shed light on understanding the behavior of excitons in WS_2 under lateral electric fields but may also provide insights relevant for high-performance optoelectronic devices based on 2D monolayer TMDs.

METHODS

Synthesis of WS_2. WS_2 monolayers and bilayers are prepared using our previously reported CVD method with sulfur and WO_3 as the precursor.[34] Sulfur and WO_3 are placed in a 1 in. quartz tube running through two furnace systems to provide two heating sections. Vaporized sulfur and WO_3 are carried by flowing argon gas to the reaction zone, where WO_3 undergoes sulfurization. High-quality and large-area WS_2 domains with atomic layer thickness are grown on Si wafers with 300 nm SiO_2 if proper parameters including temperature, Ar flow rate, and sulfur introduction time are achieved.[34]

PL and Electrical Measurement. In the photoluminescence measurement, a 532 nm diode-pumped solid-state laser is used for excitation, with powers kept to <200 μW. The laser is reflected off a dichroic beam splitter and focused to a spot size of 2 μm by a 50× ultralong working distance objective during electric-field-dependent measurements or a 10× objective lens during the temperature-dependent PL measurements on WS_2 single crystals. A hot plate is used to control the temperature of the

sample. PL spectra are collected by a custom-built confocal microscope imaging system coupled to a spectrometer with an attached CCD (Princeton Instruments Acton SP-2300 spectrometer with Princeton Instruments, PIXIS 100 CCD).

In the electrical measurements, two ultrafine W tips (Signatone, SE-T, 5 μm in diameter) are used to make direct contact with WS_2 crystals to avoid any damages or impurities introduced during the patterning process.[24] Electrical signals are powered and measured by a Keithley source meter (2400-LV). Both PL and electrical measurements are carried out under ambient conditions and room temperature.

Conflict of Interest: The authors declare no competing financial interest.

Acknowledgment. J.H.W. thanks the Royal Society for support. Z.H. thanks the CSC and the Oxford−China scholarship fund for support.

Supporting Information Available: Additional information on another example of PL enhancement from bilayer WS_2 and the evaluation of energy of electrons gained under an electric field. This material is available free of charge *via* the Internet at http://pubs.acs.org.

REFERENCES AND NOTES

1. Kim, Y.; Huang, J.-L.; Lieber, C. M. Characterization of Nanometer Scale Wear and Oxidation of Transition Metal Dichalcogenide Lubricants by Atomic Force Microscopy. *Appl. Phys. Lett.* **1991**, *59*, 3404–3406.
2. Mak, K. F.; Lee, C.; Hone, J.; Shan, J.; Heinz, T. F. Atomically Thin MoS_2: A New Direct-Gap Semiconductor. *Phys. Rev. Lett.* **2010**, *105*, 136805.
3. Radisavljevic, B.; Radenovic, A.; Brivio, J.; Giacometti, V.; Kis, A. Single-Layer MoS_2 Transistors. *Nat. Nanotechnol.* **2011**, *6*, 147–150.
4. Li, T.; Galli, G. Electronic Properties of MoS_2 Nanoparticles. *J. Phys. Chem. C* **2007**, *111*, 16192–16196.
5. Lebègue, S.; Eriksson, O. Electronic Structure of Two-Dimensional Crystals from *Ab Initio* Theory. *Phys. Rev. B* **2009**, *79*, 115409.
6. Cheiwchanchamnangij, T.; Lambrecht, W. R. L. Quasiparticle Band Structure Calculation of Monolayer, Bilayer, and Bulk MoS_2. *Phys. Rev. B* **2012**, *85*, 205302.
7. Splendiani, A.; Sun, L.; Zhang, Y.; Li, T.; Kim, J.; Chim, C.-Y.; Galli, G.; Wang, F. Emerging Photoluminescence in Monolayer MoS_2. *Nano Lett.* **2010**, *10*, 1271–1275.
8. Tongay, S.; Zhou, J.; Ataca, C.; Lo, K.; Matthews, T. S.; Li, J.; Grossman, J. C.; Wu, J. Thermally Driven Crossover from Indirect toward Direct Bandgap in 2D Semiconductors: $MoSe_2$ *versus* MoS_2. *Nano Lett.* **2012**, *12*, 5576–5580.
9. Tonndorf, P.; Schmidt, R.; Bottger, P.; Zhang, X.; Borner, J.; Liebig, A.; Albrecht, M.; Kloc, C.; Gorden, O.; Zahn, D. R. T.; et al. Photoluminescence Emission and Raman Response of Monolayer MoS_2, $MoSe_2$, and WSe_2. *Opt. Express* **2013**, *21*, 4908–4916.
10. Gutiérrez, H. R.; Perea-López, N.; Elías, A. L.; Berkdemir, A.; Wang, B.; Lv, R.; López-Urías, F.; Crespi, V. H.; Terrones, H.; Terrones, M. Extraordinary Room-Temperature Photoluminescence in Triangular WS_2 Monolayers. *Nano Lett.* **2013**, *13*, 3447–3454.
11. Perea-López, N.; Lin, Z.; Pradhan, N. R.; Iñiguez-Rábago, A.; Laura Elías, A.; McCreary, A.; Lou, J.; Ajayan, P. M.; Terrones, H.; Balicas, L.; et al. CVD-Grown Monolayered MoS_2 as an Effective Photosensor Operating at Low-Voltage. *2D Mater.* **2014**, *1*, 011004.
12. Perea-López, N.; Elías, A. L.; Berkdemir, A.; Castro-Beltran, A.; Gutiérrez, H. R.; Feng, S.; Lv, R.; Hayashi, T.; López-Urías, F.; Ghosh, S.; et al. Photosensor Device Based on Few-Layered WS_2 Films. *Adv. Funct. Mater.* **2013**, *23*, 5511–5517.
13. Lopez-Sanchez, O.; Lembke, D.; Kayci, M.; Radenovic, A.; Kis, A. Ultrasensitive Photodetectors Based on Monolayer MoS_2. *Nat. Nanotechnol.* **2013**, *8*, 497–501.
14. Feng, J.; Qian, X.; Huang, C.-W.; Li, J. Strain-Engineered Artificial Atom as a Broad-Spectrum Solar Energy Funnel. *Nat. Photonics* **2012**, *6*, 866–872.
15. Wi, S.; Kim, H.; Chen, M.; Nam, H.; Guo, L. J.; Meyhofer, E.; Liang, X. Enhancement of Photovoltaic Response in Multilayer MoS_2 Induced by Plasma Doping. *ACS Nano* **2014**, *8*, 5270–5281.
16. Lopez-Sanchez, O.; Alarcon Llado, E.; Koman, V.; Fontcuberta i Morral, A.; Radenovic, A.; Kis, A. Light Generation and Harvesting in a van der Waals Heterostructure. *ACS Nano* **2014**, *8*, 3042–3048.
17. Bernardi, M.; Palummo, M.; Grossman, J. C. Extraordinary Sunlight Absorption and One Nanometer Thick Photovoltaics Using Two-Dimensional Monolayer Materials. *Nano Lett.* **2013**, *13*, 3664–3670.
18. Jo, S.; Ubrig, N.; Berger, H.; Kuzmenko, B. A.; Morpurgo, F. A. Mono- and Bilayer WS_2 Light-Emitting Transistors. *Nano Lett.* **2014**, *14*, 2019–2025.
19. Sundaram, R. S.; Engel, M.; Lombardo, A.; Krupke, R.; Ferrari, A. C.; Avouris, P.; Steiner, M. Electroluminescence in Single Layer MoS_2. *Nano Lett.* **2013**, *13*, 1416–1421.
20. Zhang, W.; Huang, J.-K.; Chen, C.-H.; Chang, Y.-H.; Cheng, Y.-J.; Li, L.-J. High-Gain Phototransistors Based on a CVD MoS_2 Monolayer. *Adv. Mater.* **2013**, *25*, 3456–3461.
21. Yin, Z.; Li, H.; Jiang, L.; Shi, Y.; Sun, Y.; Lu, G.; Zhang, Q.; Chen, X.; Zhang, H. Single-Layer MoS_2 Phototransistors. *ACS Nano* **2012**, *6*, 74–80.
22. Desai, S. B.; Seol, G.; Kang, J. S.; Fang, H.; Battaglia, C.; Kapadia, R.; Ager, J. W.; Guo, J.; Javey, A. Strain-Induced Indirect to Direct Bandgap Transition in Multilayer WSe_2. *Nano Lett.* **2014**, *14*, 4592–4597.
23. Mak, K. F.; He, K.; Lee, C.; Lee, G. H.; Hone, J.; Heinz, T. F.; Shan, J. Tightly Bound Trions in Monolayer MoS_2. *Nat. Mater.* **2013**, *12*, 207–211.
24. Ross, J. S.; Wu, S.; Yu, H.; Ghimire, N. J.; Jones, A. M.; Aivazian, G.; Yan, J.; Mandrus, D. G.; Xiao, D.; Yao, W.; et al. Electrical Control of Neutral and Charged Excitons in a Monolayer Semiconductor. *Nat. Commun.* **2013**, *4*, 1474.
25. Ramasubramaniam, A.; Naveh, D.; Towe, E. Tunable Band Gaps in Bilayer Transition-Metal Dichalcogenides. *Phys. Rev. B* **2011**, *84*, 205325.
26. Bludau, W.; Wagner, E. Impact Ionization of Excitons in GaAs. *Phys. Rev. B* **1976**, *13*, 5410–5414.
27. Skromme, B. J.; Stillman, G. E. Impact Ionization of Excitons and Shadow Donors in InP. *Phys. Rev. B* **1983**, *28*, 4602–4607.
28. Zhang, S. K.; Santos, P. V.; Hey, R. Photoluminescence Modulation by High-Frequency Lateral Electric Fields in Quantum Wells. *Appl. Phys. Lett.* **2001**, *78*, 1559–1561.
29. Huang, H.; Dorn, A.; Nair, G. P.; Bulović, V.; Bawendi, M. G. Bias-Induced Photoluminescence Quenching of Single Colloidal Quantum Dots Embedded in Organic Semiconductors. *Nano Lett.* **2007**, *7*, 3781–3786.
30. Rothenberg, E.; Kazes, M.; Shaviv, E.; Banin, U. Electric Field Induced Switching of the Fluorescence of Single Semiconductor Quantum Rods. *Nano Lett.* **2005**, *5*, 1581–1586.
31. Baugher, B. W. H.; Churchill, H. O. H.; Yang, Y.; Jarillo-Herrero, P. Optoelectronic Devices Based on Electrically Tunable p-n Diodes in a Monolayer Dichalcogenide. *Nat. Nanotechnol.* **2014**, *9*, 262–267.
32. Pospischil, A.; Furchi, M. M.; Mueller, T. Solar-Energy Conversion and Light Emission in an Atomic Monolayer p-n Diode. *Nat. Nanotechnol.* **2014**, *9*, 257–261.
33. Ross, J. S.; Klement, P.; Jones, A. M.; Ghimire, N. J.; Yan, J.; Mandrus, D. G.; Taniguchi, T.; Watanabe, K.; Kitamura, K.; Yao, W.; et al. Electrically Tunable Excitonic Light-Emitting Diodes Based on Monolayer WSe_2 p-n Junctions. *Nat. Nanotechnol.* **2014**, *9*, 268–272.
34. Rong, Y.; Fan, Y.; Leen Koh, A.; Robertson, A. W.; He, K.; Wang, S.; Tan, H.; Sinclair, R.; Warner, J. H. Controlling Sulphur Precursor Addition for Large Single Crystal Domains of WS_2. *Nanoscale* **2014**, *6*, 12096–12103.
35. Zhao, W.; Ghorannevis, Z.; Chu, L.; Toh, M.; Kloc, C.; Tan, P.-H.; Eda, G. Evolution of Electronic Structure in Atomically Thin Sheets of WS_2 and WSe_2. *ACS Nano* **2013**, *7*, 791–797.
36. Berkdemir, A.; Gutiérrez, H. R.; Botello-Méndez, A. R.; Perea-López, N.; Elías, A. L.; Chia, C.-I.; Wang, B.; Crespi, V. H.; López-Urías, F.; Charlier, J.-C.; et al. Identification of

Individual and Few Layers of WS_2 Using Raman Spectroscopy. *Sci. Rep.* **2013**, *3*, 1755.
37. Frey, G. L.; Tenne, R.; Matthews, M. J.; Dresselhaus, M. S. Optical Properties of MS_2 (M = Mo, W) Inorganic Fullerene-like and Nanotube Material Optical Absorption and Resonance Raman Measurements. *J. Mater. Res.* **1998**, *13*, 2412–2417.
38. Fang, H.; Tosun, M.; Seol, G.; Chang, T. C.; Takei, K.; Guo, J.; Javey, A. Degenerate N-Doping of Few-Layer Transition Metal Dichalcogenides by Potassium. *Nano Lett.* **2013**, *13*, 1991–1995.
39. Schubert, E.; Gessmann, T.; Kim, J. *Light Emitting Diodes*; Cambridge University Press: Cambridge, U.K., 2006.
40. Konig, U. L. F.; Langmann, U. Temperature Distribution in Gunn Diodes and GaAs MESFET's Determined by Microphotoluminescence. *Trans. Electron Devices* **1978**, *25*, 49–55.
41. O'Donnell, K. P.; Chen, X. Temperature Dependence of Semiconductor Band Gaps. *Appl. Phys. Lett.* **1991**, *58*, 2924–2926.
42. Mitioglu, A. A.; Plochocka, P.; Jadczak, J. N.; Escoffier, W.; Rikken, G. K. J. A.; Kulyuk, L.; Maude, D. K. Optical Manipulation of the Exciton Charge State in Single-Layer Tungsten Disulfide. *Phys. Rev. B* **2013**, *88*, 245403.
43. Iveland, J.; Martinelli, L.; Peretti, J.; Speck, J. S.; Weisbuch, C. Direct Measurement of Auger Electrons Emitted from a Semiconductor Light-Emitting Diode under Electrical Injection: Identification of the Dominant Mechanism for Efficiency Droop. *Phys. Rev. Lett.* **2013**, *110*, 177406.
44. Kulyuk, L.; Dumcehnko, D.; Bucher, E.; Friemelt, K.; Schenker, O.; Charron, L.; Fortin, E.; Dumouchel, T. Excitonic Luminescence of the Br_2-Intercalated Layered Semiconductors 2H-WS_2. *Phys. Rev. B* **2005**, *72*, 075336.
45. Green, M. A. *Solar Cells: Operating Principles, Technology and System Applications*; Prentice Hall: Upper Saddle River, NJ, 1982.
46. Fox, M. *Optical Properties of Solids*; Oxford Univeristy Press: Oxford, U.K., 2001.
47. Chernikov, A.; Berkelbach, T. C.; Hill, H. M.; Rigosi, A.; Li, Y.; Aslan, O. B.; Reichman, D. R.; Hybertsen, M. S.; Heinz, T. F. Exciton Binding Energy and Nonhydrogenic Rydberg Series in Monolayer WS_2. *Phys. Rev. Lett.* **2014**, *113*, 076802.
48. Ridley, B. K.; Watkins, T. B. The Possibility of Negative Resistance Effects in Semiconductors. *Proc. Phys. Soc.* **1961**, *78*, 293–304.
49. Gunn, J. B. Microwave Oscillations of Current in III−V Semiconductors. *Solid State Commun.* **1963**, *1*, 88–91.
50. Kang, J.; Tongay, S.; Zhou, J.; Li, J.; Wu, J. Band Offsets and Heterostructures of Two-Dimensional Semiconductors. *Appl. Phys. Lett.* **2013**, *102*, 012111.
51. Zhao, W.; Ribeiro, R. M.; Toh, M.; Carvalho, A.; Kloc, C.; Castro Neto, A. H.; Eda, G. Origin of Indirect Optical Transitions in Few-Layer MoS_2, WS_2, and WSe_2. *Nano Lett.* **2013**, *13*, 5627–5634.
52. Smith, D. L.; Pan, D. S.; McGill, T. C. Impact Ionization of Excitons in Ge and Si. *Phys. Rev. B* **1975**, *12*, 4360–4366.